THE ASTROPHYSICAL JOURNAL, 435:71–78, 1994 November 1

MARKARIAN 315: A TEST CASE FOR THE ACTIVE GALACTIC NUCLEUS–MERGER HYPOTHESIS?[1]

JOHN W. MACKENTY
Space Telescope Science Institute, 3700 San Martin Drive, Baltimore, MD 21218
mackenty@stsci.edu

SUSAN M. SIMKIN
Michigan State University, Department of Physics and Astronomy, East Lansing, MI 48824-1116
simkin@grus.pa.msu.edu

RICHARD E. GRIFFITHS
Johns Hopkins University, Physics and Astronomy, 3400 North Charles Street, Baltimore, MD 21218
griffith@stsci.edu

JAMES S. ULVESTAD[2]
Jet Propulsion Lab, 4800 Oak Grove Drive, Mail Stop 301-125J, Pasadena, CA 91109
jsu@grouch.jpl.nasa.gov

AND

ANDREW S. WILSON[2]
Space Telescope Science Institute, 3700 San Martin Drive, Baltimore, MD 21218
awilson@stsci.edu

Received 1994 January 11; accepted 1994 May 3

ABSTRACT

Using the *Hubble Space Telescope* Wide Field/Planetary Camera, we have detected a diffuse continuum knot in the inner regions of the Seyfert galaxy Markarian 315. This knot may be a remnant nucleus. It is associated with a complex, ringlike structure in both the continuum and ionized gas emission. We have measured the kinematics of the ionized gas in two position angles and find velocities which are consistent with a nonaxisymmetric gravitational disturbance. The galaxy is associated with an extended ionized filament, or tidal tail, and our measurements show that the ionized gas in this feature is redshifted by up to 500 km s^{-1} in the line of sight relative to the Seyfert nucleus. This combination of morphological and kinematic features suggests that Mrk 315 has suffered a disruptive, tidal interaction which has significantly influenced regions within 1 kpc of its nucleus.

Subject headings: galaxies: individual (Markarian 315) — galaxies: interactions — galaxies: kinematics and dynamics — galaxies: Seyfert

1. INTRODUCTION

1.1. *Galaxy Mergers and Nuclear Activity*

Mergers and tidal interactions between galaxies have been studied extensively since the pioneering work of Toomre & Toomre (1972). Such galaxy-galaxy interactions provide cogent explanations for a wide variety of extreme and rare morphological features (e.g., long tails, rings, and shells). Moreover, theoretical considerations suggest that active galactic nucleus (AGN) luminosities may be fueled by tidally induced mass inflow, through a mechanism which redistributes the angular momentum of nonnuclear material and brings it closer to the nucleus (cf. Hills 1975; Gunn 1979).

The leading candidate for this fueling mechanism is some form of bisymmetric gravitational disturbance (Norman & Silk 1983; Schwarz 1985; Byrd et al. 1986; Byrd, Sundelius, & Valtonen 1987; Matsuda et al. 1987; Noguchi 1987, 1988). This may be caused by an external companion, an internal bar, or a nonaxisymmetric potential arising from a recent merger, and is expected to operate on radial scales in excess of 100–500 pc.

While most observational studies have found some statistical evidence that active nuclei are found more frequently in host galaxies with signs of recent or ongoing tidal interactions, the overall picture which emerges is confusing and sometimes contradictory. Some studies suggest that galaxies with close companions have enhanced nuclear activity (of either the AGN or the starburst type), while others find that AGNs with the largest ratio of nonthermal to starburst nuclear activity are the least likely to have a close neighboring galaxy (cf. Adams 1977; Simkin, Su, & Schwarz 1980; Petrosian 1982; Stockton 1982; Kennicutt & Keel 1984; Dahari 1984, 1985; Heckman et al. 1986; Petrosian & Turatto 1986; Bushouse 1986, 1987; Fuentes-Williams & Stocke 1988; MacKenty 1989, 1990; and the extensive review by Osterbrock 1991).

In addition, recent theoretical work points to a more complex situation in which galaxy interactions and mergers may help induce radial inflow in regions beyond 100 pc from the nucleus, but small-scale oval distortions, secondary nuclei, or bars (possibly induced by large-scale tidal interactions) and cloud-cloud collisions must play a dominant role on smaller scales (Noguchi 1987; Lin, Pringle, & Rees 1988; Shlosman, Frank, & Begelman 1989; Hernquist 1989, 1993).

In the case of AGN "feeding," some calculations suggest (Lin et al. 1988) that while the dynamical timescale at 1–2 kpc

[1] Based on observations with the NASA/ESA *Hubble Space Telescope* obtained at the Space Telescope Science Institute, which is operated by the Association of Universities for Research in Astronomy, Inc., under NASA contract NAS5-26555.

[2] Visiting Astronomer, VLA–National Radio Astronomy Observatory. NRAO is operated by Associated Universities, Inc., under contract to the National Science Foundation.

from an active galactic nucleus (and thus the duration of visible disruption) is only (5–10) × 10^6 yr, the induced "feeding" process can last for up to 10^9 yr. This implies that the chance of catching such disruption "in the act" is small and may be less than 1:100.

1.2. *Markarian 315*

This paper reports the discovery of just such a disruptive, tidal interaction in the inner 1 kpc region of the Seyfert galaxy Markarian 315 (Markarian & Lipovetskii 1971) (also II Zw 187). This object is a moderately luminous Seyfert 1.5 galaxy (Koski 1978). It has a mean H I redshift of 11,827 km s^{-1} relative to the Galactic center (Mirabel & Wilson 1984). Earlier optical work (Sargent 1970), found its optical emission-line redshift to be 11,640 km s^{-1} (significantly lower than the H I value) and $M_v = -21.6$. For this discussion we adopt a scale of 0.57 h^{-1} kpc arcsec^{-1}.

Radio frequency images of Mrk 315 show that it is a steep-spectrum source with a diffuse morphology and a total extent of 5.7 h^{-1} kpc at 20 cm (Ulvestad, Wilson, & Sramek 1981; Ulvestad & Wilson 1984). These authors note that this extended radio continuum structure is the largest in their sample of Seyfert galaxies (which typically ranged between 0.05 and 2.8 h^{-1} kpc). It is, however, consistent with an extended starburst in the galaxy (Wilson 1988).

MacKenty (1986) discovered an extraordinary, 60 h^{-1} kpc filament of ionized gas emerging from near the nucleus of Mrk 315, extending in a straight line for 45 h^{-1} kpc, then bending back in a hook to the southeast (cf. Figs. 1*a* and 1*b* of that paper). Two possible origins for this feature were proposed: a tidal interaction or a dormant radio jet. The observations reported here strongly support the idea of a tidal origin and establish Mrk 315 as an extreme example of an active galaxy with a strong tidal disruption in the gas-rich material close to its nucleus.

2. OBSERVATIONS AND REDUCTIONS

2.1. *HST Image*

Mrk 315 was observed with the *Hubble Space Telescope* (*HST*) using the Wide Field/Planetary Camera (WF/PC) (Westphal et al. 1982). This snapshot observation (W0Z10L01) was obtained as part of GO Program 3698. The details are listed in Table 1. This exposure at a scale of 43 mas pixel^{-1} shows a second, diffuse peak in proximity to the nucleus (which is located near the center of the PC 6 detector). The spacecraft pointing stability in course track guiding mode was 97 mas (measured using the star 30″ south of Mrk 315 which fell on the PC 7 detector). Both this star and the Seyfert nucleus are diffraction-limited, with the first Airy ring visible. The feature to the east is clearly not a point source, since it does not have an Airy ring (Fig. 1*a* [Pl. 1]).

The *HST* image was processed with the standard WF/PC pipeline software (see, e.g., Lauer 1989; MacKenty et al. 1992). A sunlit Earth, F785LP flat field (STScI Calibration Database ID: c1916444w.r6h) was used to correct for instrumental gain variations. The image was manually edited to remove cosmic rays by interpolation, and deconvolved using both the Lucy-Richardson algorithm (the STSDAS LUCY task) and a maximum-entropy algorithm (maximum-entropy method [MEM]) with a front end developed by Weir (1991a, b). The point-spread function (PSF) used in both cases was created with the TINYTIM optical modeling package (Burrows et al. 1991; Krist 1993). The MEM restoration is shown in Figure 1*b*.

2.2. *Ground-based Narrow-Band and Continuum Images*

Mrk 315 was observed with the University of Hawaii 2.24 m telescope at Mauna Kea Observatory (MKO) in 1983 and 1984. The observational details are presented in MacKenty (1986). The MKO images were taken under good seeing conditions but suffered image blurring (of 2″–2.″5) caused by guiding errors. Two deep, narrow-band (80 Å) images covering redshifted [O III] $\lambda\lambda$4959, 5007 and Hα and one deep, KPNO-Mould, *I*-band image were used for comparison with the *HST* image (see Table 1).

For better comparison with the *HST* image, the guiding errors were corrected, using a star at P.A. 149°, 29.″3 south-southeast of the nucleus as a PSF with the MEM restoration interface written by Weir (1991a, b). The sharpened images have PSFs with 1.″5 full width at half-maximum (FWHM) (i.e., no superresolution was attempted). The small-scale features in the resulting images were enhanced by subtracting the large-scale smooth galaxy structure, thus emphasizing both emission-line regions and regions of increased red continuum density (for example, late-type stars).

The inner regions of the narrow-band MKO images are shown in Figures 2*a*–2*c* (Plate 2). The uncorrected Hα image is reproduced in Figure 2*a*, and the guiding corrected images of Hα and [O III] in Figures 2*b* and 2*c*. Comparison of the Hα images in Figures 2*a* and 2*b* demonstrates that the complex ringlike structure in the sharpened images is not an artifact of the correction process.

The *I*-band image is shown in Figure 1*c*. The restored *HST* image, rebinned at the same scale as the MKO images, is shown in Figure 1*d* for comparison. The well-defined knot found in the *HST* observation to the east of the Seyfert nucleus, appears to be the brightest feature in a ring or armlike structure (all of the images in Figs. 1*c* and 1*d* and 2*a*–2*d* have been binned to the same resolution, 0.″42 pixel^{-1}).

The orientation and ellipticity of the galaxy's outer isophotes were measured using the method described by Jedrzejewski (1987) as implemented in STSDAS. In addition to the deep *I*-band image listed in Table 1, three separate frames in *V*,

TABLE 1

MARKARIAN 315 IMAGES

UT Date	Telescope/Instrument	Wavelength (Å)	Exposure (s)	Scale (arcsec pixel^{-1})
1984 Jun 29 12:32	UH 2.24 m TI uniphase CCD	5163–5213	6000	0.42
1984 Jun 30 12:39	UH 2.24 m TI uniphase CCD	6793–6838	4500	0.42
1984 Sep 01 08:08	UH 2.24 m TI uniphase CCD	7200–9300	600	0.42
1992 Jun 15 16:34	*HST* WF/PC	7800–10000	230	0.043

1994ApJ...435...71M

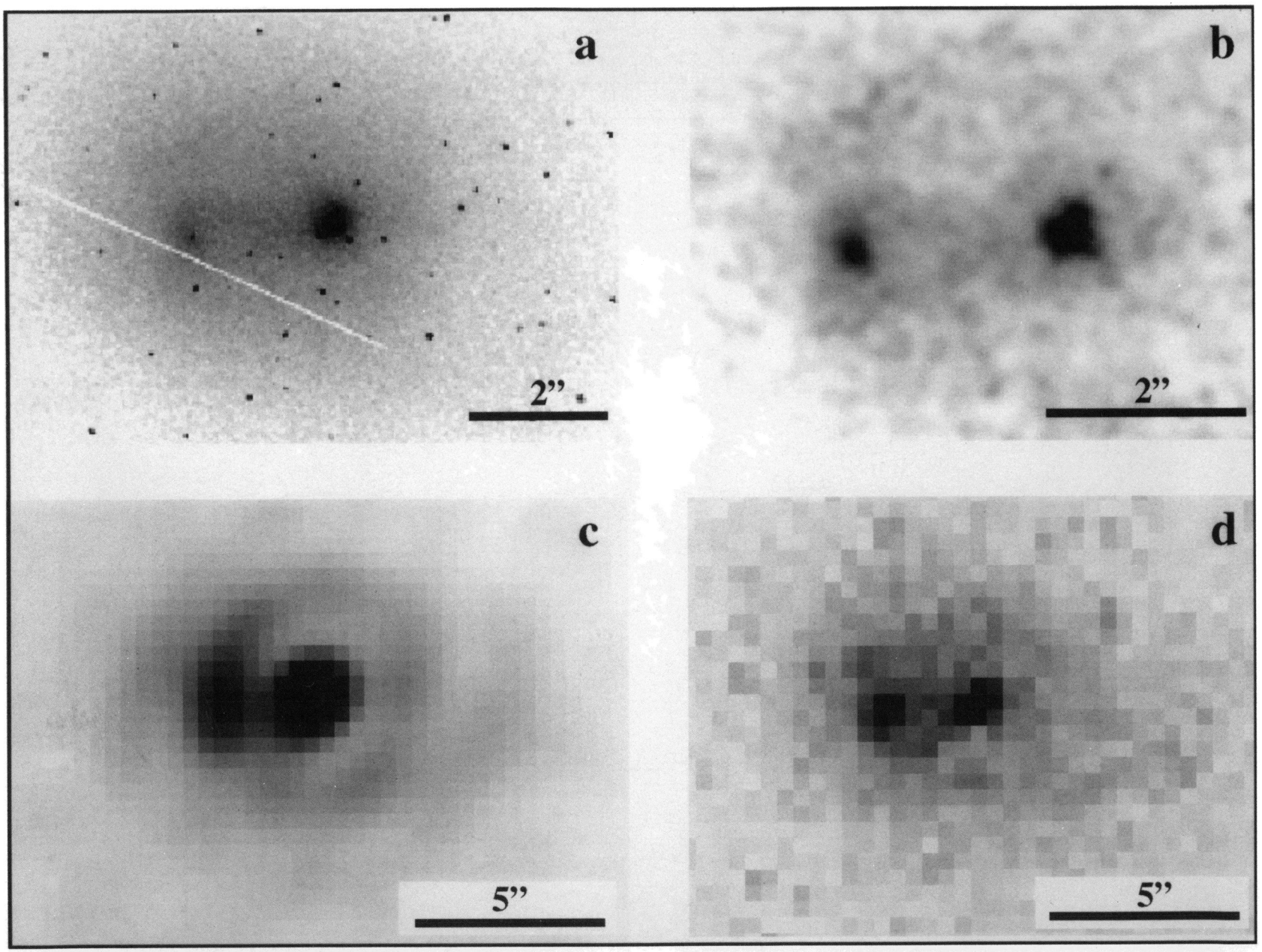

FIG. 1.—Comparison of the WF/PC F785LP image with the ground-based *I*-band image Mrk 315: (*a*) Unrestored *HST* image (before editing of cosmic-ray events), showing the point-source Seyfert nucleus and the resolved secondary knot. The diagonal white line is a bad column in the CCD detector which has been interpolated across prior to the image restoration. (*b*) Restored *HST* image. (*c*) Ground-based *I*-band image, restored to correct for guiding errors. (*d*) Restored *HST* image, binned to the same scale as the ground-based image. All images in this figure are oriented with north at the top and east to the left.

MACKENTY et al. (see 435, 72)

PLATE 1

1994ApJ...435...71M

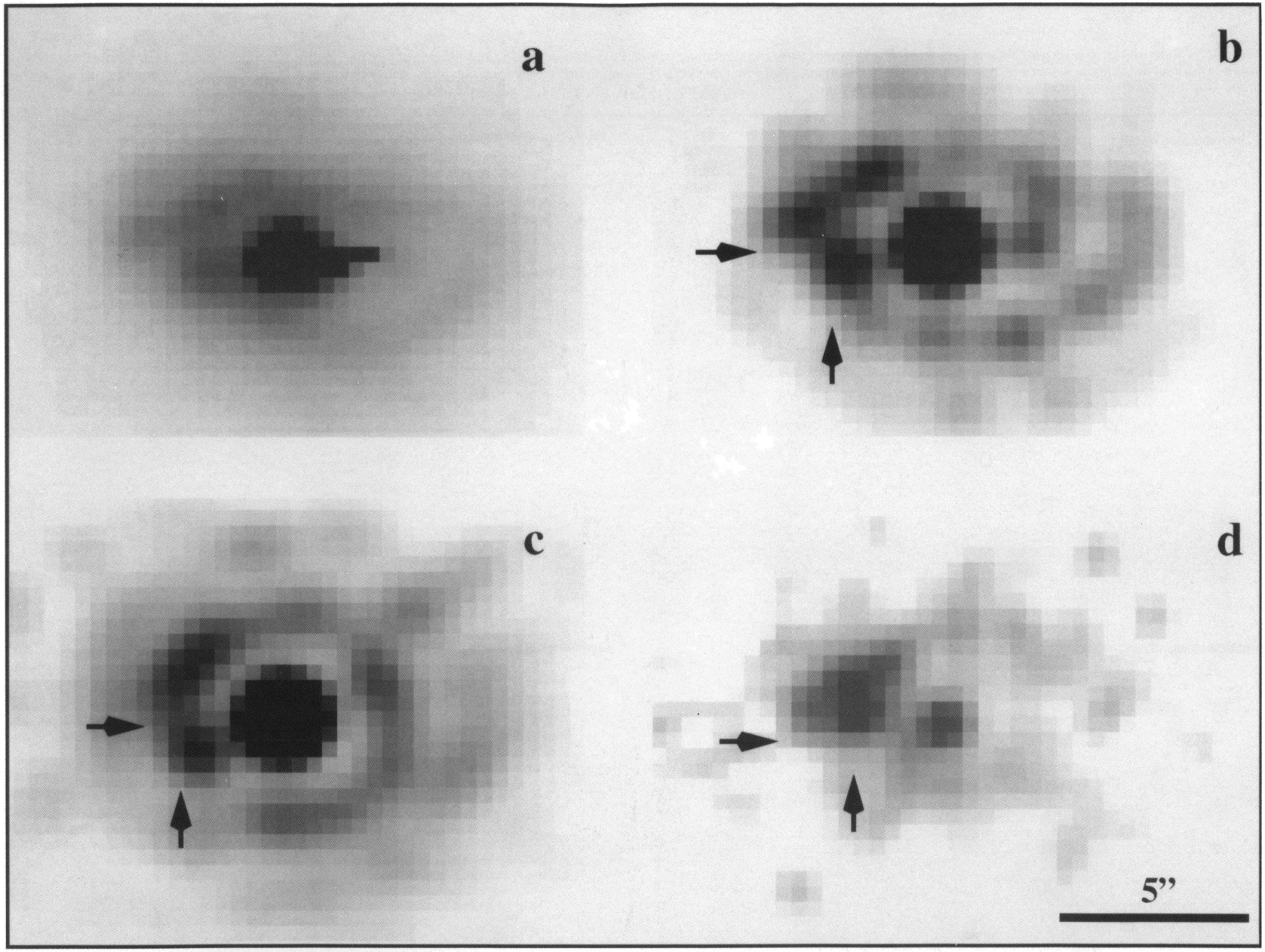

FIG. 2.—Comparison of ground-based optical and VLA radio images of Mrk 315: (*a*) Unprocessed Hα image. (*b*) Hα with guiding errors removed (see text). (*c*) [O III] with guiding errors removed. (*d*) VLA 20 cm image. Orientations are the same as in Fig. 1. All images in this figure are to scale marked in (*d*). The position of the continuum knot is marked on (*b*)–(*d*).

B, and *R* (listed in MacKenty 1986) were used for this purpose. The results give a position angle for the outer major axis of 68°.5 ± 1°.5 and (if the ellipticity is indicative of inclination) an inclination to the plane of the sky of 38°.5 ± 2°. In all cases, there was no discernible shift in the isophote centers with increasing distance from the nucleus. (The shift was less than 0".5 or 0.28 h^{-1} kpc.)

2.3. *Long-Slit Spectra*

In 1985 September, long-slit spectra were obtained using the University of Hawaii Institute for Astronomy Faint Object Spectrograph, equipped with a TI 3-phase CCD camera and a high-throughput, low-resolution grating, on the University of Hawaii 2.24 m telescope. Conditions during both nights were nonphotometric, and the observations were ended by clouds on 1985 September 19 at 11:40 UT. Four of the long-exposure spectra were positioned along the ionized gas filament at P.A. −36°. The fifth, short-exposure spectrum was taken at P.A. 0°. All spectra had the nucleus centered on a 4".7 wide slit. The scale along the slit was 0".68 pixel^{-1}. The dispersion was roughly 1.5 Å pixel^{-1}. Three of these spectra covered the wavelength region including Hβ and [O III] λλ5007, 4958 (4920–5670 Å), while the other two covered Hα, [N II] and the red [S II] lines (6570–7070 Å) (Table 2). The flat-fielded spectra were calibrated in wavelength. The rms error for the fit to this calibration was 0.25 Å in the blue and 0.15 Å in the red.

To compare the emission-line intensity distributions from the spectra with those from the narrow-band Hα and [O III] emission-line images, the spectra were averaged in wavelength over the emission line regions and an averaged "sky + galaxy continuum" component, from the emission-line–free continuum, was subtracted. The narrow-band, emission-line images were rotated by 36° and rebinned to 0".68 pixel^{-1}, and a 4".76 (7 pixel) wide strip along each column, centered on the nucleus, was averaged and the peak intensity positions shifted to the same pixel position as the peak in the intensity distributions derived from the spectra. These average profiles are plotted in Figure 3 as the log of the counts (normalized to 100,000 counts at the peak in all cases). The Hα profiles are offset from the [O III] profiles by 0.5 dex. The PSFs for the restored MKO images are plotted at the bottom. The greater relative intensity of the [O III] spectral profile (as opposed to the image profile beyond 6" to the northwest of the nucleus may be attributed to the fact that the prominent line at 5007 Å is redshifted to the edge of the narrow-band filter in this region.

Emission-line positions in each of the sky-subtracted two-dimensional spectra were measured by finding all features with total integrated flux above the continuum in excess of 10 times the continuum rms noise. Positions for these features were determined using three routines which calculate, respectively, the peak of the emission line, the center of a Gaussian fit to the excess emission above the continuum in the region of the emission line, and the centroid of this excess emission. The mean of the first two wavelength position measurements was used to calculate the emission-line redshifts. Beyond ~10" from the nucleus, the only emission lines with flux in excess of 10 times the continuum noise were the [O III] λλ4958, 5007 pair, Hα, and Hβ in the filament. In addition, the two blue spectra at P.A. −36° were shifted to a common nuclear position and co-added to improve the signal-to-noise ratio in the faint, outer [O III] line. The latter was measured manually.

TABLE 2

MKO SPECTRA

UT Date	P.A.	Exposure (s)	Region	Zero-Point (km s^{-1})
1985 Sep 17 08:02.....	0°	120	Blue	177
1985 Sep 17 10:55.....	144	1800	Blue	137
1985 Sep 17 11:53.....	144	5700	Blue	137
1985 Sep 18 08:15.....	144	3600	Red	108
1985 Sep 18 09:35.....	144	3600	Red	108

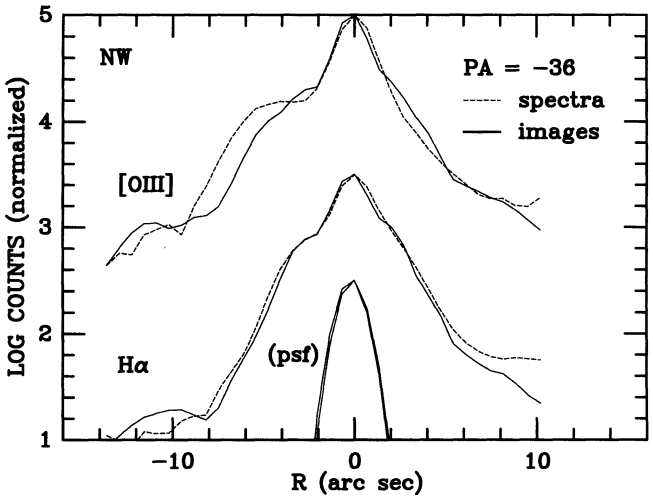

FIG. 3.—Comparison of the emission-line flux along the "filament" for the spectra and the ground-based images. The weaker signal from the [O III] interference filter probably results because the high-velocity gas is redshifted outside the filter band.

The velocity zero points for each spectrum were measured from the night-sky line [O I] λ5577 in the "blue" spectra and the OH emission bands in the "red" spectra at 6863.2, 6900.8, and 6923.9 Å (cf. Osterbrock & Martel 1992). These are listed in the last column of Table 2. However, comparison of velocities measured using different emission lines in the galaxy spectrum shows that either the gas in the inner regions of the galaxy which emits Hβ is redshifted relative to that which emits Hα (in the same line of sight), or the zero point for the red spectra derived from the OH night-sky measurements is too large (by ~100 km s^{-1}). The latter possibility is not unreasonable because the extreme width of the slit degrades the velocity resolution sufficiently to render measurements of molecular band features suspect. On the other hand, Hα and [O III] velocity measurements in the *outer* regions of the galaxy (beyond 10") are in better agreement when the red velocity zero point in Table 2 *is* applied. In the face of this ambiguity, we have chosen to incorporate the zero points for the "blue" spectra at P.A. 0° and −36° in our measured velocities from these spectra but *not incorporate* the zero points listed in Table 2 for the "red" spectra in our velocity measurements from Hα, [N II], and [S II]. However, the possibility remains that the red spectral features are systematically blueshifted with respect to the Hβ line, and this ambiguity can only be settled with more accurately calibrated measurements.

The velocity data are plotted in Figures 4 and 5. In the spectra, the emission lines of Hα and [O III] clearly break up into at least two components, the velocity system associated with the filament (marked by the dashed curve in Fig. 5) and that closer to the nucleus. The [O III] lines also have a highly blueshifted component at the nuclear position (~11,350 km

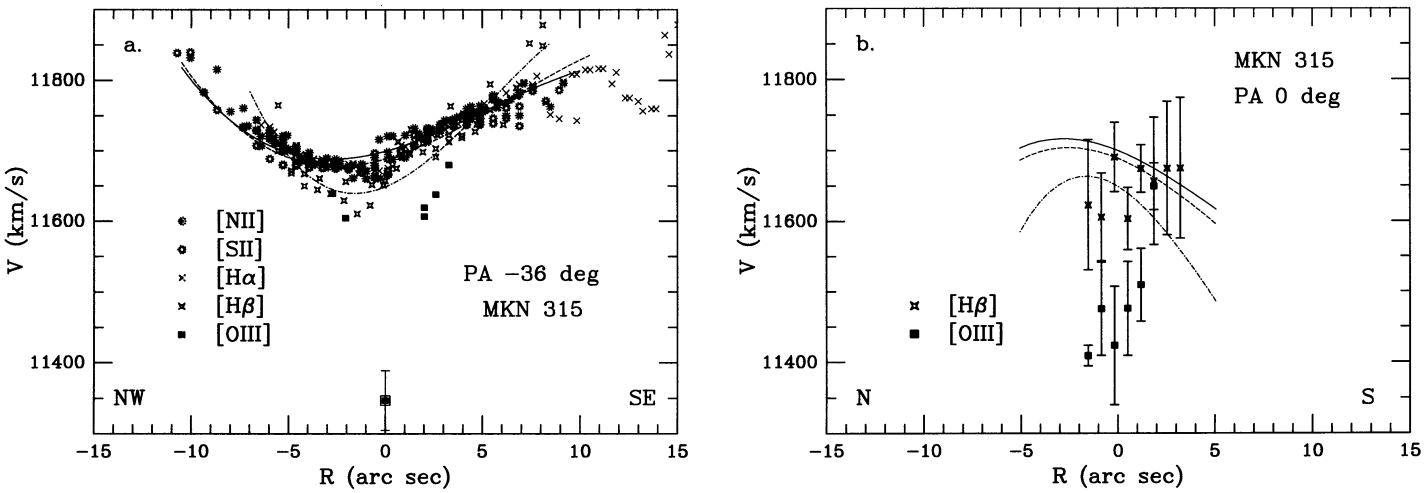

FIG. 4.—(*a*) Combined measurements for the central part of the galaxy from all four spectra at P.A. −36°. The solid and dashed curves represent, respectively, fits to the [N II] and [S II] data, while the dash-dot curve is a fit to the Hβ data. (*b*) Measurements for the short-exposure spectrum at P.A. 0°. The plotted curves are the fits from (*a*) reflected into P.A. 0° (see text).

s^{-1} in the figures). The complex nature of the velocity field can be seen in the contour plots of [O III] λ5007 in Figure 6 and the line profiles of Hα, Hβ, and [O III] λ5007 in Figure 7.

2.4. *VLA Map*

Following the discovery of the extended ionized gas filament, an improved 20 cm VLA image was obtained on 1985 February 3 (UT) with the array in the A configuration in an attempt both to detect the filament and to resolve the extended structure found earlier. A cleaned image of this data, tapered and weighted to emphasize extended features, shows no trace of the extended filament. However, an arclike structure which appears similar to that seen northwest of the secondary knot found in the *HST* image does appear in these data. This is shown in Figure 2*d* as an image made with uniform weighting and no taper. The original synthesized image had a grid spacing of 0.″25 $pixel^{-1}$ and was cleaned with a restored beam of 1.″06 × 1.″12 (at P.A. −57°.3). The image in Figure 2*d* has been rebinned to match the resolution of the MKO images (0.″42) and aligned so that the strong western emission peak in the radio coincides with the optical Seyfert nucleus. The gross similarities between the 20 cm VLA image and the ring structure in the Hα image (Figs. 2*d* and 2*b*) suggest that the extended radio continuum emission comes from the same region as the optical line emission.

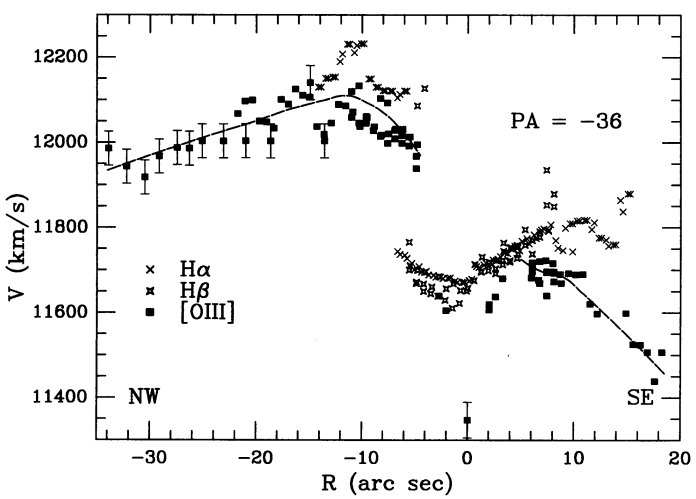

FIG. 5.—Full range of velocities in the spectra for P.A. −36°. The fit to the high-velocity data (the filament) is a second-order least-squares curve. The lower velocity data are the same as those in Fig. 4*a*.

3. ANALYSIS

3.1. *Comparison of the Images*

The diffuse peak found in the *HST* WF/PC image (Figs. 1*a* and 1*b*) is located 2.″27 east (at P.A. 95°) of the stellar Seyfert nucleus. This second peak is clearly resolved (i.e., nonstellar) with a Gaussian FWHM of 0.″66 (0.38 h^{-1} kpc). This continuum peak lies to the south of the peak in the ionized gas and 20 cm continuum (Figs 1 and 2*b*–2*d*).

At the redshift of Mrk 315, the WF/PC F785LP filter spans the wavelength region 7504–9621 Å, while the Mould *I*-band filter covers the range 6927–8947 Å. The only notable nebular emission lines in this wavelength range are an [S III] doublet at 9069, 9532 Å. Any contribution from these weak features to the broad-band F785LP and *I* filters will be small. Thus the strength of this diffuse knot in the near-IR and its small contribution to the [O III] and Hα images (Figs. 1*b* and 1*c*) imply that it comes from a collection of very red continuum sources, most likely K- and M-type stars.

The faint X-shaped linkage seen in Figure 1*b* between the diffuse knot and the Seyfert nucleus shows up in all versions of the *HST* image (both raw and processed) and appears to be real. In addition, fainter spiral or ringlike structures are present in the *HST* image at a distance of 2″–2.″5 (1–1.5 h^{-1} kpc) from the nucleus, opening toward the west (Fig 1*d*). As noted in § 2.3, the diffuse knot actually coincides with the brightest feature in a ring surrounding the Seyfert nucleus seen in the MKO *I*-band image (Fig. 1*c*). The brighter of the spiral/ring features in the *HST* image (opening to the north of the diffuse knot) appears to be part of this ring. The more prominent appearance of the ring in the MKO *I*-band image is most likely the result of the higher signal-to-noise ratio in the MKO image.

The ring in the *I* images also appears in the Hα and [O III] images (Figs. 2*b* and 2*c*), but with slightly different relative

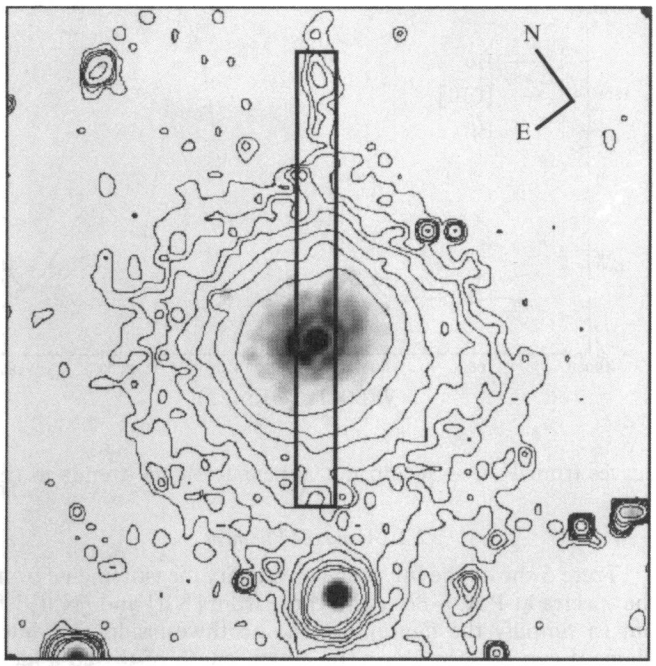

FIG. 6a

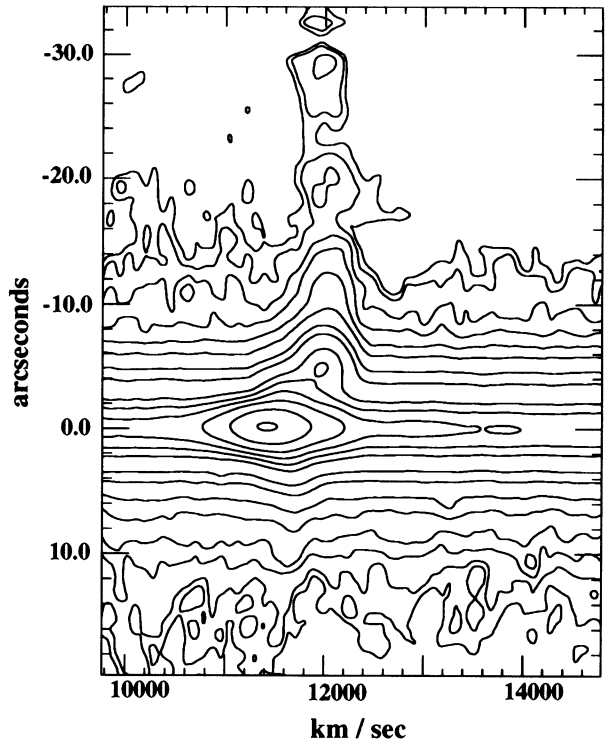

FIG. 6b

FIG. 6.—(*a*) Projection of the spectrograph slit onto the [O III] image of the galaxy, with the inner region in gray scale and the outer region as contour overlays. The image is rotated by 36°. (*b*) Intensity contours of [O III] λ5007 as a function of position along the slit and velocity, from the blue co-added spectra in P.A. −36° (see text).

intensities. The diffuse knot seen in the *HST* image appears to coincide with a gap in the Hα and [O III] rings (see the markers in Figs 2*b* and 2*c*). The fainter spiral feature seen in the southwest of the *HST* image lies just to the outside of a strong, knotty arc seen in the Hα image (Fig. 2*b*). When superposed, other detailed features in the three images show similar morphologies but different relative intensities. For example, the inner ring appears more circular in the [O III] image (Fig. 2*c*) than in the Hα image (Fig. 2*b*), because there is a gap in the latter (slightly to the south of west) and a prominent Hα knot just outside the ring (due east of the nucleus) which also seems to be part of the 20 cm continuum feature. The inner base of the filament seen by MacKenty (1986) is prominent in the [O III] image (pointing toward the letter "c" in Fig. 2*c*) but scarcely visible in the Hα image.

The coincidence of the strong Hα emission with the radio continuum feature to the east of the nucleus (and the relatively weaker [O III] emission in that area) support the conclusion that Mrk 315 hosts a starburst of large spatial extent. This agrees with the suggestion of Ulvestad et al. (1981) that diffuse radio emission in Seyfert galaxies such as Mrk 315 can be associated with starbursts (also see Wilson 1988). The diffuse knot (presumably composed of late-type stars) seen in the *HST* image lies adjacent to this gaseous complex, and we speculate that this knot is somehow responsible for the starburst.

3.2. *Comparison of the Spectra and the Narrow-Band Images*

Figure 6*a* shows the projected spectrograph slit on the [O III] image of the galaxy. The inner ring and filament are shown in gray scale, while the other extent of the galaxy and filament are shown as contour overlays. The image is rotated by 36°, putting the slit direction along the *y*-axis. The width of the slit covers not only the nucleus but also most of the inner ring. This overlap, and the consequent blending of the emission features from different regions, makes the spectral interpretation complex. The length of the slit plotted in Figure 6*a* covers the region of the galaxy where the emission lines were strong enough to measure velocities (the actual spectra extend well beyond this to the southwest).

Figure 6*b* shows intensity contours of [O III] λ5007 (from the blue co-added spectra. The knot located ∼5″ to the northwest of the nucleus at a redshift greater than 12,000 km s^{-1} corresponds to the base of the long, extended filament, where it terminates at the circumnuclear ring. This feature is visible in all of the emission lines in the spectra (Hα, Hβ, [O III] λλ4959, 5007, [N II], and [S II]) but is only strong enough to measure in [O III], Hα, and Hβ. Although the spectograph slit encompassed the continuum knot seen in the *HST* image and the adjacent Hα knot (∼2″.3 from the nucleus; cf. Figs. 6*a* and 1*c*–1*d*), there is no kinematically distinct feature at this position.

3.3. *Kinematics*

3.3.1. *Interior to the Ring*

The kinematics of the interior of the galaxy derived from our spectra are shown in Figures 4*a* and 4*b*. The solid and dashed curves represent, respectively, fits to the [N II] and [S II] data at P.A. −36°. The dash-dot curve is a fit to the Hβ data at that position angle. In Figure 4*b* these curves have been converted into the velocity distribution along P.A. 0°, using the values for the inclination to the plane of the sky and the line of nodes

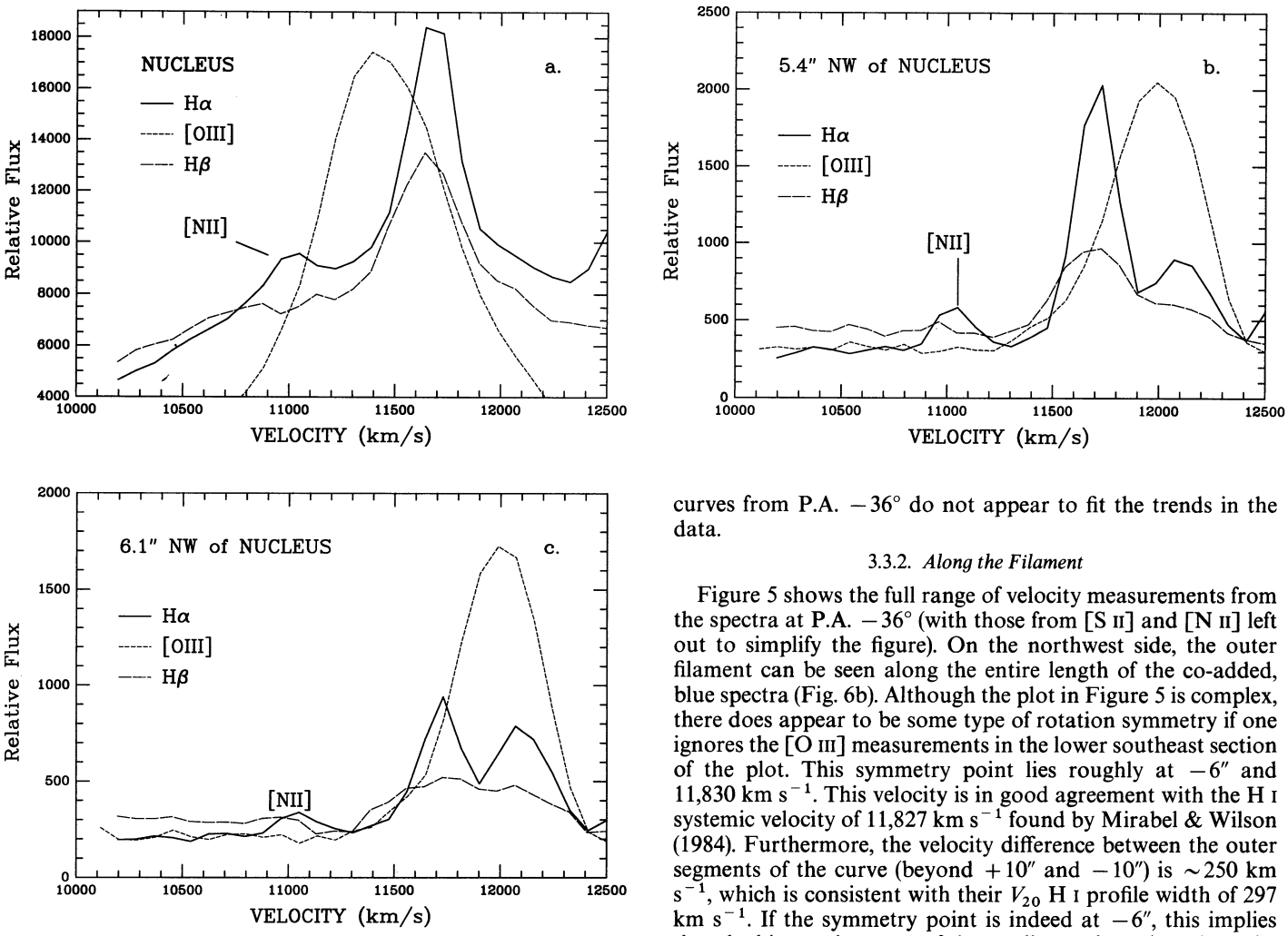

FIG. 7.—Relative flux plotted as a function of velocity from Hα, Hβ, and [O III] λ5007, showing the velocity change from the nucleus (*a*) to the point where the "filament" terminates just outside the ring in (*b*) and (*c*).

determined from the direct images (§ 2.2). The error bars on the measurements plotted in Figure 4*b* indicate the uncertainties arising from the very low signal-to-noise ratio of this spectrum.

Figures 4*a* and 4*b* show two notable features. First, the [O III] measurements in the nucleus (in both Figs 4*a* and 4*b*) are blueshifted by ~ 325 km s^{-1} relative to those for Hβ, Hα, [N II], and the red [S II] lines (11,350 km s^{-1} versus 11,675 km s^{-1}). (The boxed-in point at zero radius in Fig. 4*a* is the mean of the four [O III] measurements [4959 and 5007 Å on two spectra] and their associated errors.) This blueshift is dramatically illustrated in Figure 7*a*, where the line profiles are plotted. In this figure there is a suggestion of an even more blueshifted component in the Hβ line at 11,150 km s^{-1}, but this cannot be confirmed in the Hα profile because it overlaps with [N II] λ6548. Second, the shape of the curve in Figure 4*a* is not that of a normal "rotation curve." Although it is roughly symmetric about the region of the nucleus, it does not show symmetry about the systemic velocity. This discrepancy also shows up in the difference between the projection into P.A. 0° of the fitted curves in P.A. −36° and the actual data (Fig. 4*b*). Although the data at P.A. 0° are of poor quality, the projected curves from P.A. −36° do not appear to fit the trends in the data.

3.3.2. *Along the Filament*

Figure 5 shows the full range of velocity measurements from the spectra at P.A. −36° (with those from [S II] and [N II] left out to simplify the figure). On the northwest side, the outer filament can be seen along the entire length of the co-added, blue spectra (Fig. 6b). Although the plot in Figure 5 is complex, there does appear to be some type of rotation symmetry if one ignores the [O III] measurements in the lower southeast section of the plot. This symmetry point lies roughly at −6″ and 11,830 km s^{-1}. This velocity is in good agreement with the H I systemic velocity of 11,827 km s^{-1} found by Mirabel & Wilson (1984). Furthermore, the velocity difference between the outer segments of the curve (beyond +10″ and −10″) is ~ 250 km s^{-1}, which is consistent with their V_{20} H I profile width of 297 km s^{-1}. If the symmetry point is indeed at −6″, this implies that the kinematic center of the gas lies at the point where the filament terminates just outside the inner ring (see Figs. 6*a* and 6*b*). In this case, the "rotation curve" in the inner regions of Mrk 315 shown in Figure 4*a* is simply one cusp of the turnover point for the entire system, and its peculiar shape reflects this fact.

4. DISCUSSION

The most likely picture which emerges from the present observations is that the diffuse knot seen in the *HST* image of Mrk 315 is the nuclear remnant of a recently captured galaxy. Its core size ($\sim 0.4\ h^{-1}$ kpc) is consistent with this picture. The circumnuclear arc or ring seen in the [O III] and Hα images is consistent with the stellar density enhancements and induced star formation which can be produced by a captured, orbiting nuclear mass in the regions including and adjacent to its orbit (Byrd, Smith, & Miller 1984). Finally, the extensive starburst seen in Hα and 20 cm continuum trailing the diffuse knot is what one would expect to find in gas clouds compressed by such a strong gravitational disturbance.

The possible shift in position between the kinematic center and the Seyfert nucleus noted in § 3.3.2 also supports this capture hypothesis. The agreement between the systemic velocity of this center (as defined by the outer velocities at P.A. −36°) and that found by Mirabel & Wilson (1984) for the H I in this galaxy suggests that there is a large cloud of neutral

hydrogen associated with the extended, ionized filament. It seems reasonable to postuate that the velocities in this cloud of neutral gas represent the disturbed remnants of the postcapture gas and that the kinematic center of mass of the composite system will be different from the position of the Seyfert nucleus.

The strongly blueshifted (~ 325 km s^{-1}) [O III] lines in the Seyfert nucleus of this object are more problematic. Wilson & Baldwin (1985) have noted the presence of blueshifted nuclear [O III] lines (~ 170 km s^{-1}) in the Seyfert galaxy NGC 2110 and have associated this with a shift in the kinematic center from the Seyfert nucleus of ~ 220 pc. On the other hand, Walker (1968) and Ulrich (1973) have measured radial outflows in clouds of ionized gas of up to 700 km s^{-1} in the nearby Seyfert galaxies NGC 4151 and NGC 1068, some of which are blueshifted. Finally, Rubin (1993) has recently shown that the nearby, non-Seyfert galaxy NGC 4826, which has both prograde and retrograde nested gas disks (Braun, Walterbos, & Kennicutt 1993) has emission-line velocities in its inner disk which are systematially low with respect to its systemic velocity in a manner similar to those seen here for Mrk 315. She interprets this as most likely due to outflow which is somehow associated with the merging gas systems. Thus the blueshifted emission in Mrk 315 may also be an indirect signature of a merger.

There remains the question of the filament. Its nondetection at 20 cm excludes the possibility of a radio jet. The morphology of the filament resembles those modeled as tidal tails in interacting galaxies, but its strong emission in the highly ionized [O III] lines differentiates it from those tidal tails which are primarily old stars. Hernquist (1993) has recently reported on models which produce infalling gas streamers with star formation as part of the merger of gas-rich systems, and this might be an example of such a phenomenon. In this case, the ionization source for the gas in the filament will be hot, young stars, which should be visible on a blue *HST* image. Alternatively, the filament could be a short-lived "wake" left behind a bow shock formed by the passage of the galaxy's nucleus through the neutral gas. The cooling time of shock-ionized gas produced by the passage of a nuclear core through the neutral gas of column density $\leq 10^{19}$ cm^{-2} would be greater than the travel time of the knot through the gas if the inclination of the filament to the line of sight is $\leq 55°$ (with the observed velocity difference of ≈ 350 km s^{-1}.) This more transient shock ionization could be distinguished from that induced by hot stars by obtaining calibrated measurements of diagnostic emission lines from the red, blue-green, and near-ultraviolet.

5. SUMMARY

The features seen in Mrk 315 are consistent with an interpretation of the secondary continuum knot as a recently captured galaxy remnant. They are also symptomatic of the type of gravitational forcing which leads to mass inflow toward the nucleus (see Osterbrock 1991 for a review). Thus this object may provide strong support for the hypothesis that galaxy interactions provide a mechanism for stimulating nuclear activity.

We believe this object provides a rare example of an AGN "caught in the act" of the initiation stage of tidally induced feeding. The timescale for this type of close (1 kpc) nuclear capture is quite short [on the order of $(5–10) \times 10^6$ yr; Lin et al. 1988]. Thus we expect objects similar to Mrk 315 to be rare. It therefore may well prove an excellent laboratory for testing detailed models of AGN activity.

Support for this work was provided by NASA through grant GO05-70600 from the Space Telescope Science Institute, which is operated by the Association of Universities for Research in Astronomy, Inc., under NASA contract NAS5-26555. The optical data analysis was done with support from NSF AST-89-14567 (to S. M. S.). A portion of this work was carried out by the Jet Propulsion Laboratory, California Institute of Technology, under contract with the National Aeronautics and Space Administration. J. W. M. and A. S. W. are grateful to the University of Hawaii for allocation of telescope time. A. S. W. appreciates the hospitality of the University of Hawaii Institute for Astronomy during a sabbatical visit. We wish to acknowledge the assistance of Alan Stockton in the use of his spectrograph, Bob Hlivak for his support of the CCD cameras, and the invaluable assistance of the UH telescope operators and day crew.

REFERENCES

Adams, T. F. 1977, ApJS, 33, 19
Braun, R., Walterbos, R. A. M., & Kennicutt, R. C., Jr. 1993, Nature, 360, 442
Burrows, C. J., Holtzman, J. A., Faber, S. M., Bely, P. Y., Hasan, H., Lynds, C. R., & Schroeder, D. 1991, ApJ, 369, L21
Bushouse, H. A. 1986, AJ, 91, 255
———. 1987, ApJ, 320, 49
Byrd, G., Smith, B. F., & Miller, R. 1984, ApJ, 286, 62
Byrd, G., Sundelius, B., & Valtonen, 1987, A&A, 171, 16
Byrd, G., Valtonen, M., Sundelius, B., & Valtaoja, L. 1986, A&A, 166, 75
Dahari, O. 1984, AJ, 89, 966
———. 1985, AJ, 90, 1771
Fuentes-Williams, T., & Stocke, J. 1988, AJ, 96, 1235
Gunn, J. E. 1979, in Active Galactic Nuclei, ed. C. Hazard & S. Mitton (Cambridge: Cambridge Univ. Press), 213
Heckman, T. M., Smith, E. P., Baum, S. A., van Breugel, W. J. M., Miley, G. K., Illingworth, G. D., Bothun, G. D., & Balick, B. 1986, ApJ, 311, 526
Hernquist, L. 1989, Ann. NY Acad. Sci., 571, 190
———. 1993, in Proc. Conf. on Mass-Transfer Induced Activity in Galaxies, ed. I. Shlosman (Cambridge: Cambridge Univ. Press), in preparation
Hills, J. G. 1975, Nature, 254, 295
Jedrzejewski, R. I. 1987, MNRAS, 225, 747
Kennicutt, R. C., & Keel, W. C. 1984, ApJ, 279, L5
Koski, A. T. 1978, ApJ, 223, 56
Krist, J. 1993, in ASP Conf. Ser. 52, Astronomical Data Analysis and Software Systems II, ed. R. J. Hanisch, R. J. V. Brissenden, & J. Barnes (San Francisco: ASP), 536
Lauer, T. R. 1989, PASP, 101, 445
Lin, D. N. C., Pringle, J. E., & Rees, M. J. 1988, ApJ, 328, 103
MacKenty, J. W. 1986, ApJ, 308, 571
———. 1989, ApJ, 343, 125
———. 1990, ApJS, 72, 231
MacKenty, J. W., et al. 1992, Hubble Space Telescope Wide Field/Planetary Camera Instrument Handbook (Baltimore: STScI)
Markarian, B. E., & Lipovetskii, V. A. 1971, Astrofizika, 7, 511
Matsuda, T., Inoue, M., Sawada, K., Shima, E., & Wakamatsu, K. 1987, MNRAS, 229, 295
Mirabel, I. F., & Wilson, A. S. 1984, ApJ, 227, 92
Noguchi, M. 1987, MNRAS, 228, 635
———. 1988, A&A, 203, 259
Norman, C., & Silk, J. 1983, ApJ, 266, 502
Osterbrock, D. E. 1991, Rep. Prog. Phys., 54, 579
Osterbrock, D. E., & Martel, A. 1992, PASP, 104, 76
Petrosian, A. R. 1982, Astrofizika, 18, 548
Petrosian, A. R., & Turatto, M. 1986, A&A, 163, 26
Rubin, V. C. 1993, ApJ, in press
Sargent, W. L. W. 1970, ApJ, 160, 405
Schwarz, M. P. 1985, MNRAS, 212, 677
Shlosman, I., Frank, J., & Begelman, M. 1989, Nature 338, 45
Simkin, S. M., Su, H.-J., & Schwarz, M. P. 1980, ApJ, 237, 404
Stockton, A. 1982, ApJ, 257, 33
Toomre, A., & Toomre, J. 1972, ApJ, 178, 623
Ulrich, M.-H. 1973, ApJ, 181, 51

Ulvestad, J. S., & Wilson, A. S. 1984, ApJ, 278, 544
Ulvestad, J. S., Wilson, A. S., & Sramek, R. A. 1981, ApJ, 247, 419
Walker, M. F. 1968, ApJ, 151, 71
Weir, N. 1991a, in Proc. ESO Workshop 38, ed. P. J. Grosbøl & R. H. Warmels (Garching: ESO), 115
———. 1991b, in Proc. 10th Int. Workshop on Maximum Entropy and Bayesian Methods, ed. W. T. Grandy & L. H. Schick (Dordrecht: Kluwer), 275
Westphal, J. A., et al. 1982, in The Space Telescope Observatory, ed. D. N. B. Hall (NASA CP-2244), 28
Wilson, A. S. 1988, A&A, 206, 41
Wilson, A. S., & Baldwin, J. A. 1985, ApJ, 289, 124